Research Square

Preprints are preliminary reports that have not undergone peer review.
They should not be considered conclusive, used to inform clinical practice,
or referenced by the media as validated information.

Enhanced Teleconnection between El Niño and Northern South China Sea Shelf Winter SST during Positive Atlantic Multidecadal Oscillation

Zhaoyun Wang
Hainan Tropical Ocean University
Mingpan Qiu
Hainan Tropical Ocean University
Yanyan Wang
Hainan Tropical Ocean University
Yimin Zhang
zym_ocean@126.com

Hainan Tropical Ocean University https://orcid.org/0009-0000-7448-2450
Xiaoju Pan
Hainan Tropical Ocean University
Guosheng Zhang
Hainan Tropical Ocean University
Dongliang Shen
Hainan Tropical Ocean University
Ruili Sun
Zhejiang University
Wenjing Dong
Hainan Tropical Ocean University

Research Article

Keywords: South China Sea, SST, Atlantic Multidecadal Oscillation, El Niño, western North Pacific anticyclone

Posted Date: May 21st, 2026

DOI: https://doi.org/10.21203/rs.3.rs-9578578/v1

License: This work is licensed under a Creative Commons Attribution 4.0 International License.
Read Full License

Enhanced Teleconnection between El Niño and Northern South China Sea Shelf Winter SST during Positive Atlantic Multidecadal Oscillation

Zhaoyun Wang[1], Mingpan Qiu[1], Yanyan Wang[1], Yimin Zhang[1*], Xiaoju Pan[1], Guosheng Zhang[1], Dongliang Shen[1*], Ruili Sun[2], Wenjing Dong[1]

[1] Yazhou Bay Innovation Institute/College of Marine Science and Technology, Hainan Tropical Ocean University, Sanya, Hainan Province, 572022, China

[2] Hainan Institute of Zhejiang University, Zhejiang University, Sanya, Hainan Province, 572022, China

***Corresponding authors**: zym_ocean@126.com (https://orcid.org/0009-0000-7448-2450); shendl@hntou.edu.cn (https://orcid.org/0009-0007-6023-000X)

Acknowledgments This research was supported jointly by the Natural Science Foundation of Hainan Province (NO.426MS0193), National Natural Science Foundation of China (NO.42266005), Scientific Research Foundation of Hainan Tropical Ocean University (NO.RHDRC202322,RHDRC202103) and Special Program of Hainan Province for Academician Innovation Platform (NO. YSPTZX202507).

ABSTRACT

Sea surface temperature (SST) on the northern South China Sea (NSCS) shelf exerts substantial controls over local marine ecosystems and socioeconomic conditions, while El Niño typically elevates winter SST there. However, the teleconnection between El Niño and NSCS shelf winter SST exhibits strong multidecadal variability. Through observational and reanalysis datasets, this work reveals that the teleconnection is

significantly enhanced during the positive phase of the Atlantic Multidecadal Oscillation (AMO). A positive AMO drives convective enhancement over the North Atlantic which intensifies the climatological zonal SST gradient across the tropical Pacific by combining tropical and mid-latitude pathways. This altered background condition forces a westward shift in the core of El Niño and the consequent anomalous western North Pacific anticyclone (WNPAC). Furthermore, the westward-shifted WNPAC weakens the cyclonic gyre in the NSCS, leading to significant warm advection along the western boundary which serves as the leading contributor for the enhanced SST warming over the NSCS shelf. Finally, a self-developed empirical model is employed to substantially improve the winter SST forecast skill on the NSCS shelf by adopting suitable Niño indices as predictors under different AMO phases. Our findings on the AMO as a key modulator of Pacific-Asian climate interactions provide a valuable path for improving regional climate prediction and projection.

Key words: South China Sea, SST, Atlantic Multidecadal Oscillation, El Niño, western North Pacific anticyclone

Article Highlights:

- The enhanced teleconnection between El Niño and NSCS shelf winter SST occurs during the positive AMO phase.
- A westward-shifted WNPAC during the positive AMO phase strengthens the teleconnection, driving significantly enhanced winter SST warming on the NSCS shelf.
- Positive AMO intensifies the climatological zonal SST gradient across the tropical Pacific through tropical and mid-latitude pathways, forcing a westward shift in the core of El Niño and the consequent anomalous WNPAC.

1. Introduction

Sea surface temperature (SST), a crucial thermodynamic parameter in air-sea coupling, exhibits pronounced multi-scale variability that serves as a pivotal fingerprint of climate change and profoundly influences marine ecosystems and socioeconomic activities (Wernberg et al. 2013; Smith et al. 2021). Under global warming, the South China Sea (SCS), as a critical part of the Indo-Pacific Warm Pool and a key junction of tropical-subtropical air-sea interactions, has emerged as an increasingly influential regulator of Asian climate (Tang et al. 2020; Wang et al. 2021; Lin et al. 2024). Within the SCS, the northern shelf region, as an important transition zone between the continent and open ocean, stands out for its exceptional ecological, navigational and socioeconomic importance (Wang et al. 2022). Unraveling the evolution and mechanism of SST anomalies on the northern SCS (NSCS) shelf is essential not only for understanding climate variability across East and Southeast Asia, but also for improving regional climate prediction, ecosystem conservation, and sustainable marine development.

On the NSCS shelf, winter SST is primarily governed by the East Asian Winter Monsoon which exacerbates the ocean cooling effect initiated by the seasonal minimum in solar radiation (Wyrtki et al. 1961). Meanwhile, the sharp zonal SST gradient is predominantly modulated by the cold advection associated with the Guangdong Coastal Current (GCC) (Fig. 1a) (Shi et al. 2002; Wong et al. 2003; Zhang et al. 2021). Beyond seasonal variability, the interannual fluctuations of winter SST over the NSCS are largely driven by El Niño-Southern Oscillation (ENSO), primarily through its modulation of the western North Pacific anticyclone (WNPAC) or cyclone (Zhang et al. 1996; Klein et al. 1999; Wang et al. 2000). During El Niño winters, the anomalous warm SST in across the

tropical central and eastern Pacific acts as a potent atmospheric heat source, forcing an anomalous low-tropospheric cyclonic circulation to its west via classical Gill-type dynamical adjustment (Gill et al. 1980). Subsequently, anomalous northeasterly winds on the northwestern side of this anomalous cyclonic anomaly reinforce the prevailing trade winds across the western equatorial Pacific, thereby enhancing surface evaporation and promoting sea surface cooling. The resulting cold SST anomalies further function as a negative heat source, suppressing atmospheric convection and generating an anomalous anticyclone over the western North Pacific through the atmospheric Rossby wave propagation (Zhang et al. 1996; Wu et al. 2017). Then the anomalous southwesterly or southeasterly winds associated with the western side of the WNPAC weaken the prevailing northeasterly winds, reducing latent heat loss and inducing significant sea surface warming over the NSCS (Wang et al. 2006; Xiao et al. 2020). Correspondingly, the anomalous WNPAC weakens the wintertime climatological cyclonic ocean gyre, which reduces cold advection driven by the SCS western boundary current and further intensifies SST warming over the NSCS (Liu et al. 2004; Seow et al. 2019).

Despite significant advances in understanding ENSO-NSCS SST teleconnections, accumulating evidence indicates that the teleconnection between El Niño and NSCS winter SST exhibits pronounced multidecadal instability. For instance, the teleconnection between El Niño and the winter cold tongue over the NSCS strengthened notably during the periods 1963-1976 and 1999-2012 (Wang et al. 2025a). This multidecadal enhancement is considered to be modulated by the negative phase of the Pacific Decadal Oscillation (PDO) that alters the structure and strength of the Walker and Hadley circulations. Further studies have confirmed that the negative PDO amplifies the

magnitude of El Niño-induced anomalous WNPAC, thereby inducing warmer SST anomalies across the SCS via both oceanic (e.g., advection) and atmospheric (e.g., wind-driven heat flux anomalies) pathways (Duan et al. 2025; Wang et al. 2025b). However, this work reveals that the teleconnection between El Niño and NSCS shelf winter SST is essentially uncorrelated with the PDO ($r \approx 0$). The multidecadal variability of this teleconnection and its underlying physical processes remain to be further explored.

Beyond the PDO, the Atlantic Multidecadal Oscillation (AMO) stands as another key low-frequency pattern that regulates large-scale global climate variability (Schlesinger et al. 1994; Enfield et al. 2001). Accompanied by warm or cold SST anomalies across the North Atlantic, AMO exerts a pronounced cross-basin spillover effect on both the North Pacific (Knight et al. 2006; Sun et al. 2017) and the Indo-Pacific region (McGregor et al. 2014; Kucharski et al. 2015). Specifically, during the positive AMO phase, the associated North Atlantic warm SST anomalies modulate the background thermal and dynamical conditions in the tropical Pacific and Indian Oceans through two key cross-basin atmospheric teleconnection pathways: a tropical pathway that directly influences equatorial circulation (Xue et al. 2025) and an extratropical pathway that propagates signals through mid-latitude circulation anomalies (Sun et al. 2017; Wang et al. 2025c). In response to positive AMO phases, the central Pacific tends to experience SST cooling, whereas the Indo-Pacific basin undergoes simultaneous warming (Xue et al. 2025). Importantly, the altered background SST in the tropical Pacific linked to the positive AMO acts to suppress ENSO amplitude by modifying the thermocline feedback and the atmospheric forcing (Gong et al. 2020; Xue et al. 2022; Zhao et al. 2022; Xu et al. 2023). A weakened ENSO amplitude further suppresses tropical Pacific convection, thereby

115 attenuating the WNPAC intensity. Whereas the AMO-ENSO amplitude relationship has
116 been widely recognized in previous studies, a critical unresolved question persists:
117 whether the AMO modulates the teleconnection between El Niño and NSCS shelf winter
118 SST. Resolving this knowledge gap is not only essential for advancing our understanding
119 of multidecadal variability in regional SST responses to ENSO forcing but also of great
120 importance for improving the predictability of local climate extremes and guiding
121 science-based coastal adaptation strategies. Using observational and reanalysis datasets,
122 this study demonstrates that the AMO indeed modulates this teleconnection, with a
123 notably stronger link during positive AMO phases.

124 2. Data and methods

125 The monthly SST data utilized in this study are obtained from the Hadley Centre Sea
126 Ice and Sea Surface Temperature (HadISST) dataset (Rayner et al. 2003). For cross-
127 validation purposes, four additional SST datasets are employed for comparison: the
128 Extended Reconstructed SST dataset (ERSST) (Huang et al. 2017), the Optimum
129 Interpolation SST (OISST) dataset (Reynolds et al. 2007), the Kaplan SST dataset
130 (Kaplan et al. 1998) and the fifth generation ECMWF reanalysis for the global climate
131 and weather (ERA5) dataset (Hersbach et al. 2020). In addition, monthly sea level
132 pressure (SLP), surface wind, surface heat flux, total precipitation, total cloud cover,
133 vertical pressure velocity, and zonal/meridional winds are derived from ERA5. Monthly
134 ocean currents and temperature data are extracted from the Simple Ocean Data
135 Assimilation (SODA) system, version 2.2.4 (Carton et al. 2008). The analysis period
136 spans 1940-2024, with the exception of SODA data, which terminate in 2010. All data
137 anomalies (relative to the 1940-2023 climatology, or 1940-2010 for SODA data) are

detrended to remove global warming signals. Winter refers to the December-February (DJF) period throughout this study.

An El Niño event is defined as the 3-month running mean of the Niño-3.4 index exceeds 0.5 °C for five consecutive months. The AMO index is derived from area-averaged North Atlantic SST anomalies within the domain of 0°-60°N, 80°W-0° (Dai et al. 2015). An 11-year low-pass filtering procedure is applied to extract dominant multidecadal signals.

Correlation, regression, and partial correlation analyses are employed to investigate the multidecadal variability of the teleconnection between El Niño and NSCS shelf SST. Statistical significance of analytical results is assessed using a two-tailed Student's t-test. Wavelet analysis (Torrence and Compo 1998) and spectral analysis (Percival and Walden 1993) are applied to decadal variation of NSCS shelf SST anomalies and AMO index. An autoregressive integrated moving average (ARIMA) model of order (3,1,3) (Box et al. 2015) and a local-level state-space model with a Kalman filter (Durbin et al. 2012) are used to estimate trends and uncertainties. To quantify the relative roles of atmospheric and oceanic processes to the SST variability on the NSCS shelf, a mixed-layer heat budget analysis is performed (Liu et al. 2021; Xiao et al. 2020).

$$\frac{\partial T_m}{\partial t} = \frac{Q_{net}}{\rho C_P H} - u \cdot \frac{\partial T_m}{\partial x} - v \cdot \frac{\partial T_m}{\partial y} - w \frac{\partial T_m}{\partial z} + R \quad (1)$$

In Equation (1), the terms from left to right correspond to the tendency of mixed layer temperature, net surface heat flux, zonal heat advection, meridional heat advection, vertical entrainment, and the residual term, respectively. Q_{net} comprises shortwave radiation, longwave radiation, latent heat flux, and sensible heat flux, where a positive

value indicates a downward heat flux. The symbols u, v, w and T_m represent the monthly averaged current components and temperature in the mixed layer, respectively. The density of seawater is taken as ρ=1027 kg/m^3 , and the specific heat capacity as Cp=4007 J °C^{-1} · kg^{-1}.

To evaluate the predictive skill of Niño-3, Niño-3.4, and Niño-4 indices for winter SSTA on the NSCS shelf, this study compares traditional linear regression with a 3-year moving window regression approach. The latter method fits regression models within a fixed-width window that advances through the time series, making it particularly suitable for capturing time-varying relationships in non-stationary data (Schrunner et al. 2023). The predictive ability of each Niño index is evaluated by comparing the root mean square error (RMSE). The analysis is divided into three sub-periods: P1 (1940-1962), N (1963-1998), and P2 (1999-2023). For period N, the predictive skills of Niño-3 and Niño-3.4 indices are compared; for periods P1 and P2, those of Niño-4 and Niño-3.4 are compared. Significant SSTA are defined as those exceeding ±0.6σ of the regional SST anomalies series during 1940–2023.

3. Results

3.1 *Multidecadal modulation of AMO on the teleconnection between El Niño and NSCS shelf winter SST*

Time series of winter NSCS shelf SST and Niño-3.4 index during 1940-2023 are illustrated in Figure 1b based on the HadISST dataset. Although prominent 2-7 year interannual variability is detected in NSCS shelf SST, its simultaneous correlation with Niño-3.4 index is relatively modest ($r=0.35$, $p<0.05$). To characterize the teleconnection between El Niño and NSCS shelf winter SST, 21-year sliding correlation analyses are presented in Figure 1c. Distinct multidecadal oscillations are identified in the correlation, which shows weak during 1960-1990 and enhances markedly in other decades. These multidecadal variability of the teleconnection between El Niño and NSCS shelf winter SST are well synchronized with AMO phase ($r=0.66$, $p<0.05$). Robust consistencies can be reproduced when alternative window widths are adopted. In comparison, a relatively weak negative correlation is detected between the sliding correlation and PDO variability ($r=-0.37$, $p<0.1$, not shown in this study).

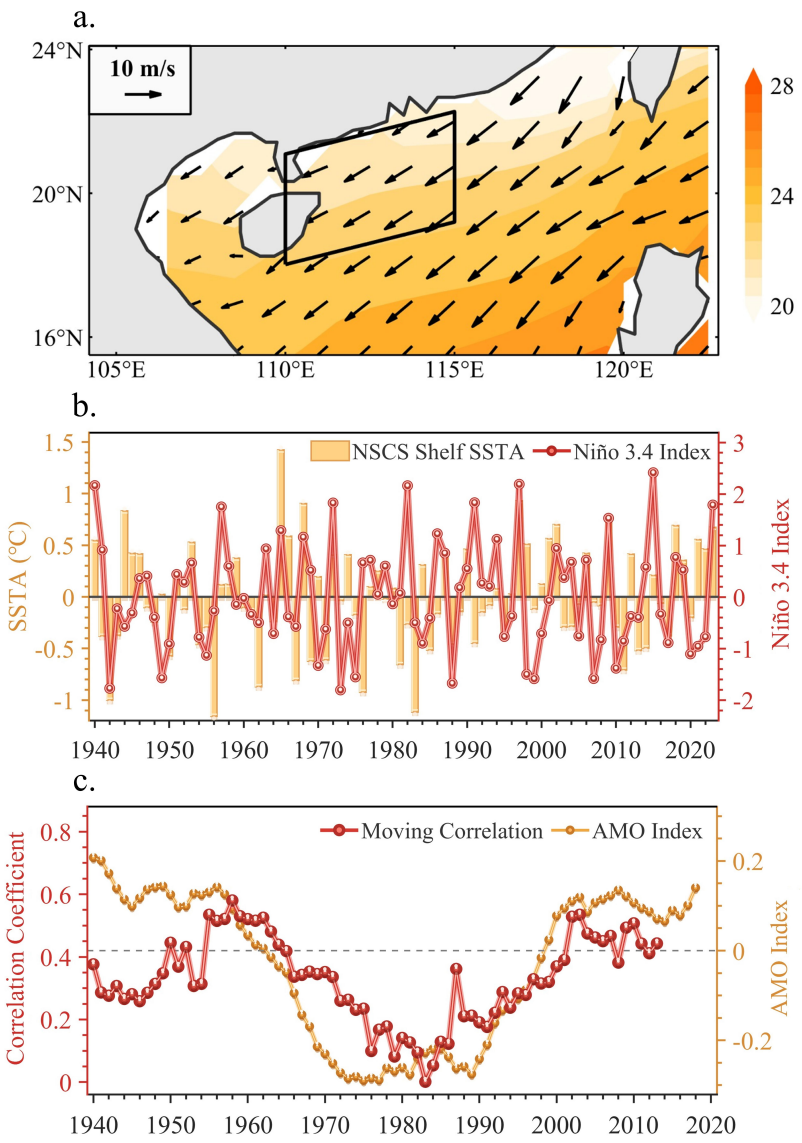


Fig. 1 Relationship between the El Niño–Northern South China Sea (NSCS) shelf winter SST teleconnection and the Atlantic Multidecadal Oscillation (AMO). (a) Climatological mean winter (DJF) sea surface temperature (SST; °C) and surface wind (m/s) derived for the period 1940-2023. The black box denotes the NSCS shelf. (b) Time series of winter SSTA on the NSCS shelf (bars; ℃) and the Niño-3.4 index (red curve) spanning 1940-2023. (c) 21-year sliding correlation coefficient between El Niño and NSCS shelf winter SST (hereinafter referred to as R_EN_NSCS for convenience, red curve) and 11-year low-pass filtered normalized AMO index (yellow line).

Four different methods reveal the teleconnection between ENSO-NSCS shelf and its linkage with the AMO. It can be seen that the state-space model extracts a continuous physical trajectory which is similar with the moving correlation(Fig. 2a), and the ARIMA(3,1,3) model predicts the post-2010 decline (Fig. 2b), both results consistently demonstrate that the teleconnection between El Niño and NSCS shelf winter SST is a robust physical process rather than stochastic noise. Wavelet analyses firstly identify a prominent 40-70 multidecadal oscillation concurrently shared by the teleconnection between El Niño-NSCS shelf and the AMO index (Fig. 2c, d). This finding is corroborated by spectral analysis (Fig. 2e), which displays highly consistent multidecadal peaks with within the 40-70 year band. Figure 2f displays the correlation map between ENSO-NSCS shelf winter SST teleconnection and the global decadal SST anomalies during 1940-2018. It can be seen that notable positive correlation dominate the North Atlantic basin, suggesting a robust linkage between the teleconnection of ENSO-NSCS shelf variability and the AMO. Accordingly, observational analysis suggests prominent multidecadal variability in the teleconnection between ENSO-NSCS shelf, which show remarkable relativity with AMO.

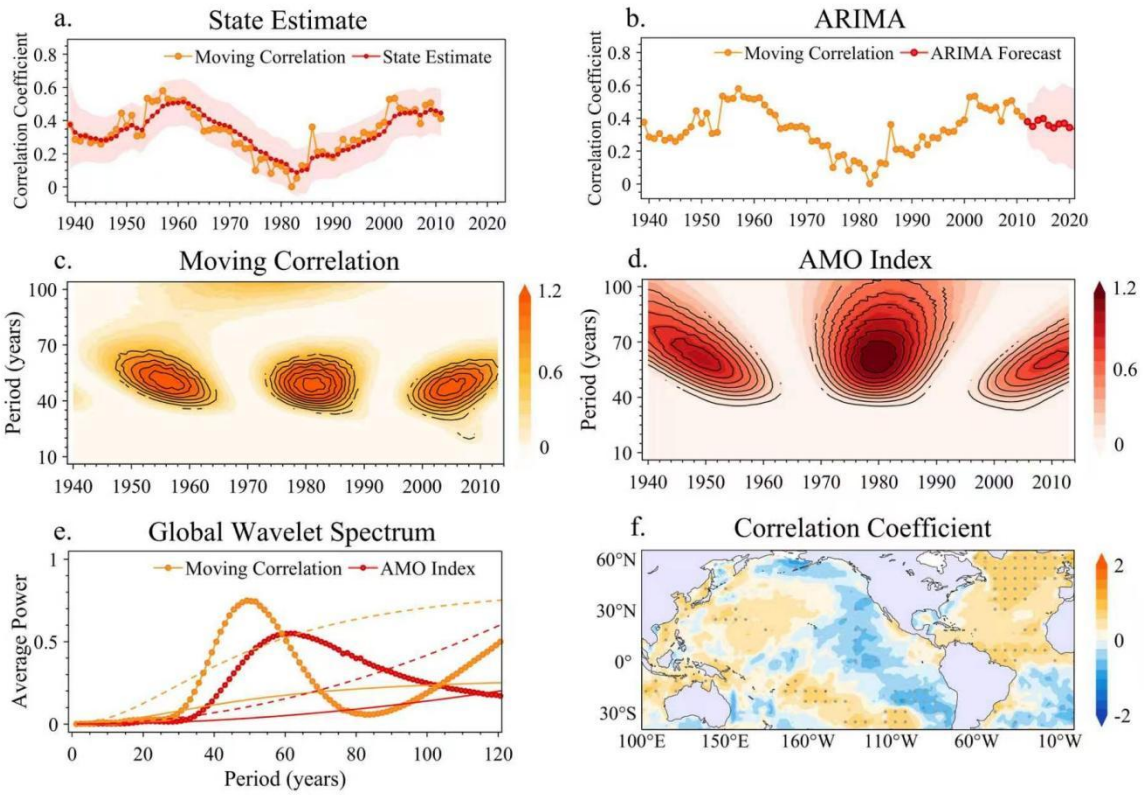


Fig. 2 Coherent multidecadal variability between the El Niño-NSCS shelf winter SST teleconnection and the AMO. (a) State-space model fitting using the Kalman filter. The orange curve denotes R_EN_NSCS, and the red curve denotes the estimated smooth component. Shading indicates the 95% confidence level.(b) Autoregressive integrated moving average (ARIMA) model fitting. The orange curve corresponds to the identical time series presented in Fig. 2a. The red curve shows the fitted values. Shading indicates the 95% confidence level. (c, d) Continuous wavelet power spectra of R_EN_NSCS and the AMO index, respectively. The black contours indicate values above the 95% confidence level. (e) Global wavelet power spectra analysis of R_EN_NSCS and the AMO index. The solid curve represents the red noise background spectrum, while the dashed curve marks the 95% statistical confidence threshold of the power spectral results. (f) Correlation map between R_EN_NSCS and the decadal annual SST anomalies during 1940-2018. Stippling indicates correlations that are statistically significant at the 99% confidence level.

229 To further examine the impact of AMO on the teleconnection between El Niño and
230 NSCS shelf winter SST, we performed a regression of NSCS shelf SSTA against the
231 Niño-3.4 index separately for positive and negative AMO phases (Fig. 3). Stronger and
232 more significant warm NSCS shelf SSTA is observed during positive AMO phases (Fig.
233 3a-e). In contrast, these warm anomalies become weaker and insignificant during
234 negative AMO phases (Fig. 3f-j). Notably, the contrast of the teleconnection between El
235 Niño and NSCS shelf winter SST between positive and negative AMO phases remain
236 robust across multiple SST datasets (Fig. 3k-o). Specifically, the magnitudes of winter
237 SSTA on the NSCS shelf during positive and negative AMO phases are comparable
238 across different datasets, ranging from 0.1 to 0.2 °C, demonstrating that the present
239 results are not sensitive to dataset choices. Collectively, the multidecadal variability of
240 the teleconnection between El Niño and NSCS shelf winter SST are substantially
241 modulated by AMO, with enhanced teleconnections in positive AMO phases and
242 attenuated in negative phases.

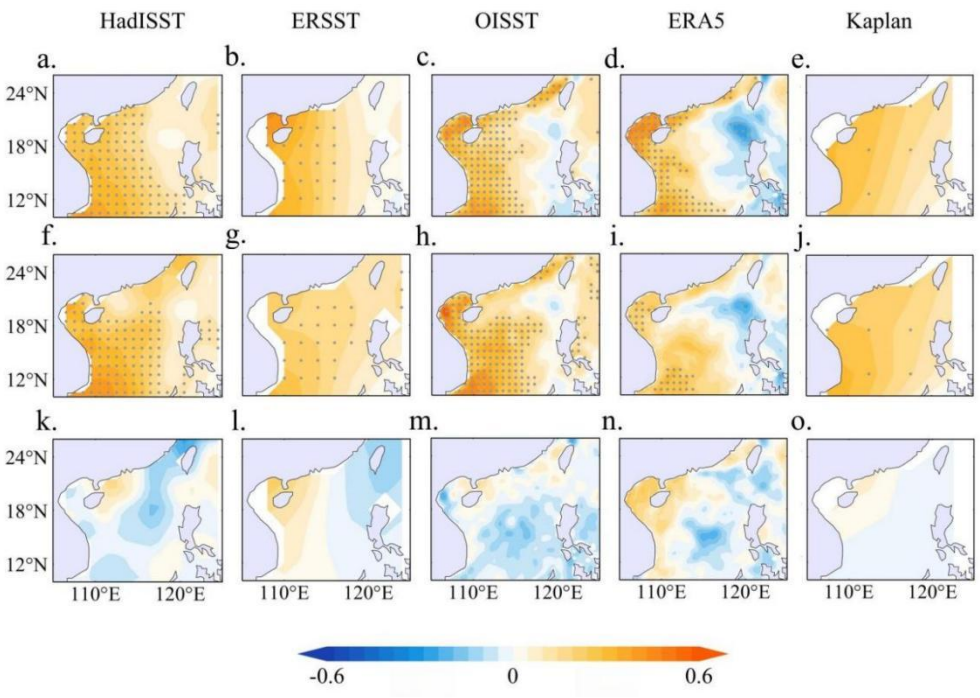


Fig. 3 Differences in the teleconnection between NSCS shelf winter SST and El Niño during positive and negative phases of AMO. (a–e) Regressed anomalies of winter SST (shading; °C) over the NSCS shelf on Niño-3.4 index under positive AMO, based on data from HadISST, ERSST, OISST, ERA5, and Kaplan. (f-j) As in (a-e), but corresponding to the negative AMO phase. (k-o) As in (a-e), but corresponding to the difference between the positive and negative AMO phases (namely positive minus negative phase results). In (a-o), Stippling highlights regions where anomalies are statistically significant at the 95% confidence level.

3.2 *Thermodynamic Processes*

The underlying processes responsible for the modulation of AMO on the multidecadal variability of the teleconnection between El Niño and NSCS shelf winter SST are further examined via mixed-layer heat budget analysis according to Equation (1) during different AMO phases (Fig. 4). In El Niño year, strong (weak) positive horizontal oceanic heat advection anomaly on the NSCS shelf is associated with strengthened (weakened) the teleconnection between El Niño and NSCS shelf winter SST (Fig. 4a)

during the positive (negative) AMO phases, and these multidecadal variations arise primarily from anomalous northward SCS western boundary currents forced by El Niño. The spatial patterns of anomalous anticyclonic gyre shift northward in positive AMO phases to allow anomalous warm water reaching the NSCS shelf (Fig. 4b), while the gyre weakens and retreats eastward for a distance of 10-15° in negative AMO phases (Fig. 4c), preventing warm water from reach the NSCS shelf. Meanwhile, the net surface heat flux exerts a comparatively subordinate contribution to the AMO-dependent difference in El Niño-induced NSCS shelf SST anomalies, and its changes are primarily dominated by latent heat flux and shortwave radiation (Fig. 5).

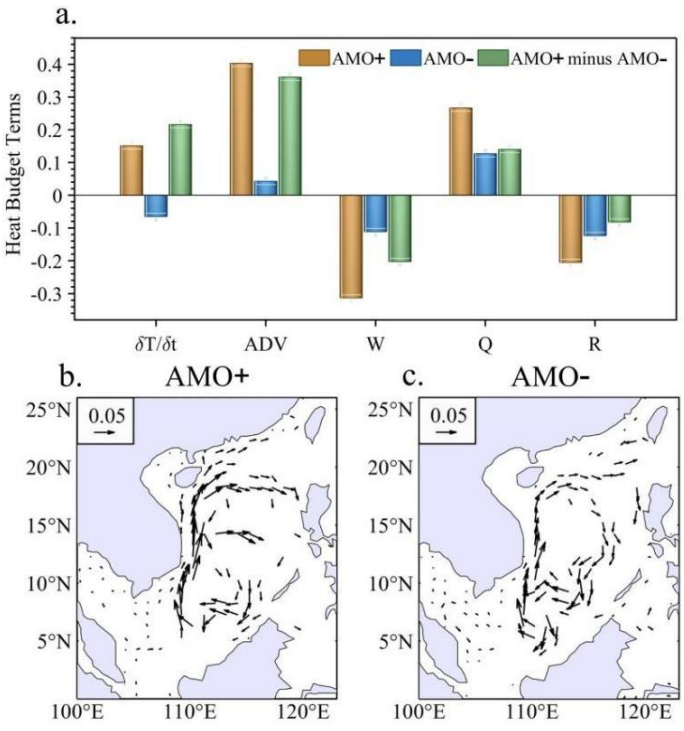


Fig. 4 Heat budget disparities on the NSCS shelf during El Niño years between positive and negative AMO phases. (a) Comparison of winter heat budget terms (δT/δt, ADV, W, Q, R; units:℃ month^{-1}) averaged over the NSCS shelf during El Niño years, separated by AMO phase. (b, c) Regression of mixed layer current (m s^{-1}) against the Niño-3.4 index during positive (b) and negative (c) AMO phases.

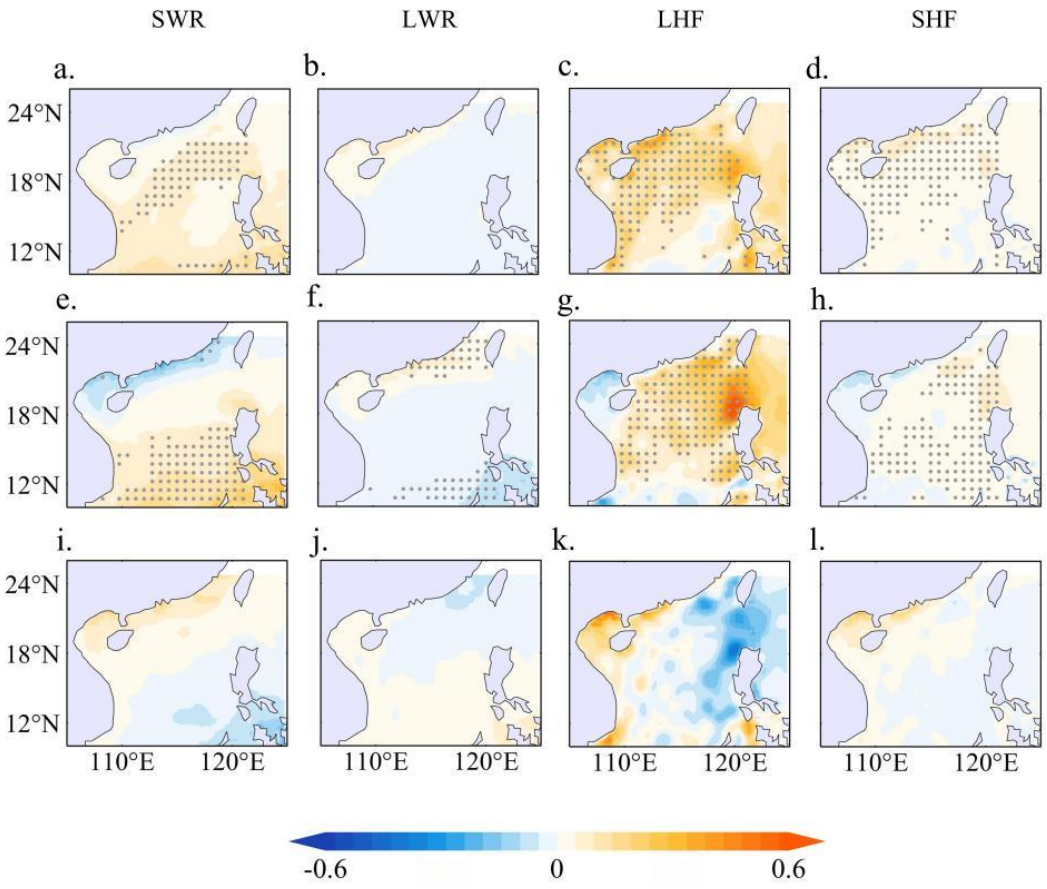


Fig. 5 As in Fig. 3, but for (a, e, i) shortwave radiation (SWR), (b, f, j) longwave radiation (LWR), (c, g, k) latent heat flux (LHF), and (d, h, l) sensible heat flux (SHF) from the ERA5 dataset. Unit:W m^{-2}. Stippling highlights regions where anomalies are statistically significant at the 95% confidence level.

3.3 *The underlying mechanism of the tropical Atlantic-Pacific pathway*

Accompanying the reduced intensity of ENSO-induced WNPAC during positive AMO phases (Fig. 6), the remote climate impacts imposed on the NSCS shelf are unexpectedly strengthened (Fig. 3). There by, it seems that the weakened WNPAC intensity alone cannot account for the enhanced teleconnection between El Niño and NSCS shelf winter SST, and that other factors must be involved. Further analysis identifies the zonal position of the WNPAC as the dominant factor. During positive AMO

phases, the El Niño forced WNPAC shifts westward remarkably, with anticyclonic centre migrating from offshore Philippine during negative AMO phase to Philippine island. Such zonal shift is synchronously accompanied by consistent variations of SLP and precipitation anomaly.

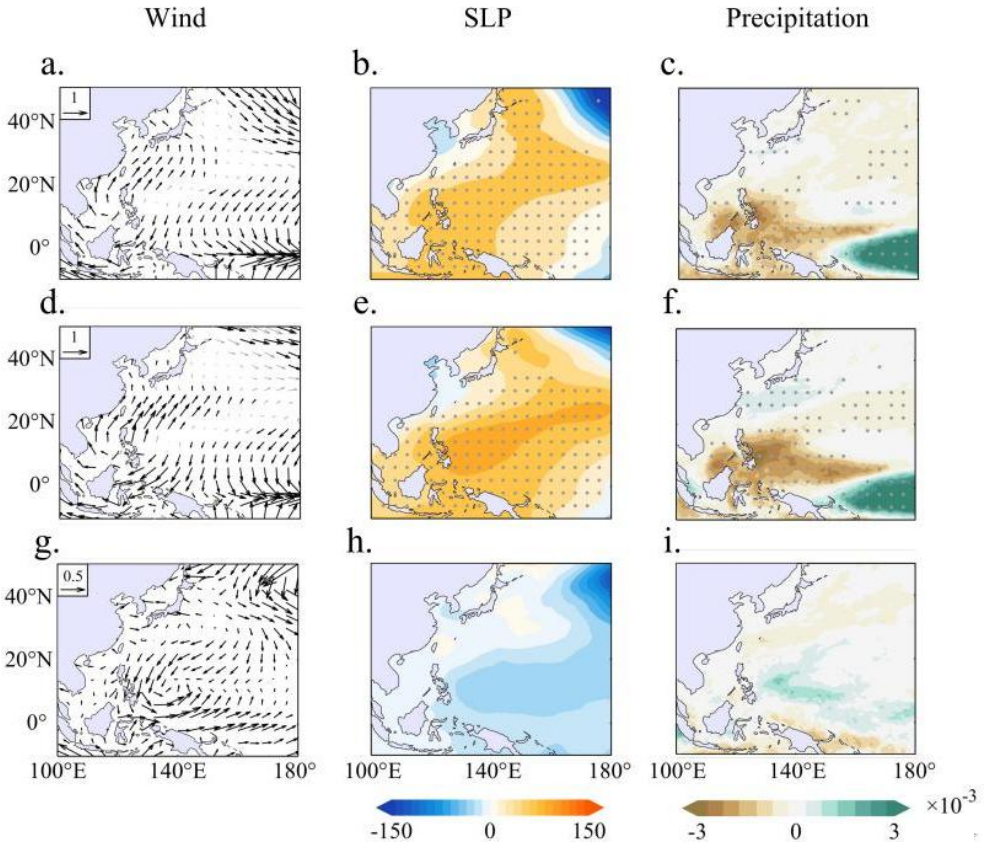


Fig. 6 As in Fig. 3, but corresponding to (a, d, g) surface wind vectors (m s^{-1}; only vectors significant at the 95% confidence level are displayed), (b, e, h) sea level pressure (SLP; shading; hPa), and (c, f, i) precipitation (shading; m day^{-1}) from the ERA5 dataset. Stippling denotes anomalies significant at the 95% confidence level for the shaded fields (SLP and precipitation).

The robust westward shift of WNPAC is further verified by the longitudes distributions of maximum SLP, geopotential height and wind stress curl (Fig. 7). Wind stress curl maxima concentrate near 120°E across both AMO phases, with only slight westward deviations in positive phases. For SLP field, the anomaly centre locates at

~122°E in positive AMO, approximately 6° west relative to negative phases, with extreme signals extending toward 100°E. The difference is more pronounced for geopotential height, whose dominant centre shifts a full 10° westward.

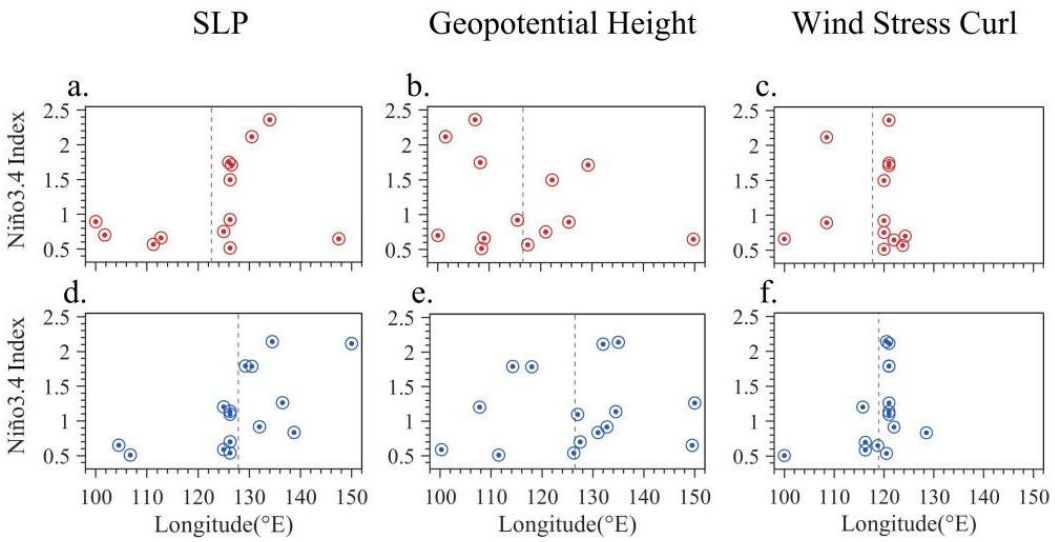


Fig. 7 Zonal distribution of the El Niño-induced western North Pacific anticyclone under different AMO phases. Scatter plots of the maximum SLP during El Niño years under positive (a) and negative (d) AMO phases; the dashed line indicates the mean value. (b, e) As in (a, d), but for 500 hPa geopotential height. (c, f) As in (a, d), but for the absolute value of wind stress curl.

The westward shift of the El Niño-induced WNPAC during positive AMO phases constitutes the key mechanism underlying the significantly warmer on the NSCS shelf. During the positive AMO phase, the El Niño-induced WNPAC undergoes a westward displacement, which in turn drives the anomalous upper-layer anticyclonic gyre to extend westward over the NSCS (Fig. 4b). This configuration drives northeastward oceanic currents with strong positive horizontal heat advection, dominating the pronounced SST warming on the shelf. Meanwhile, the westward-shifted WNPAC exerts a significant suppressing effect on local convection: it reduces near-surface specific humidity, thereby lowering evaporation efficiency and leading to a positive downward latent heat flux

anomaly; concurrently, it decreases cloud cover, which enhances the incoming shortwave radiation. Both of these processes act as secondary contributors to the higher NSCS shelf SST warming. In contrast, during the negative AMO phase, the El Niño-induced WNPAC is located farther eastward. As a result, the associated anomalous anticyclonic gyre fails to extend to the NSCS shelf, precluding the establishment of effective warm advection. Additionally, the eastward-displaced WNPAC does not suppress convection or evaporation on the NSCS shelf, thus preventing the occurrence of sustained local warming. Collectively, these results demonstrate that the phase of the AMO modulates the zonal position of the El Niño-forced WNPAC, which in turn determines the occurrence and intensity of NSCS shelf SST warming by modulating horizontal heat advection and local surface heat flux.

To further unravel the mechanism through which ENSO teleconnectively forces the zonal shift of the WNPAC under different AMO phases, we conducted a comprehensive investigation of the monthly modulation effects of the AMO on Pacific background states, including SST, SLP and wind fields (Fig. 8). In November, tropical Atlantic warming alters the Walker circulation, thereby exciting anomalous subsidence over the central-eastern Pacific. In the lower troposphere, the descending air masses exhibit divergent flow, which induces surface convergence over the western tropical Pacific and thereby forms a high-pressure centre that suppresses convection and reshapes the Pacific Walker circulation, accompanied by anomalous surface easterly winds across the central-western Pacific. This circulation anomaly exerts two distinct effects: over the central-eastern Pacific, enhanced evaporation, Ekman pumping and a shallower thermocline collectively lead to a cooling effect (San et al. 2024; Luongo et al. 2025), whereas over the western

Pacific, intensified zonal heat transport and a deepened thermocline contribute to significant warming. Crucially, the western Pacific warming subsequently fuels a strong Bjerknes feedback, amplifying the anomalous easterlies and establishing a stable positive feedback loop. This Atlantic-driven, La Niña-like anomaly peaks in December and persists through February and is crucial for the westward displacement of the WNPAC during the positive phase of AMO. Heat budget analysis (Fig. 9a) further confirms that zonal heat advection associated with the anomalous low-level easterlies dominates the western Pacific warming, overwhelming the counteracting effects of thermocline deepening and atmospheric forcing.

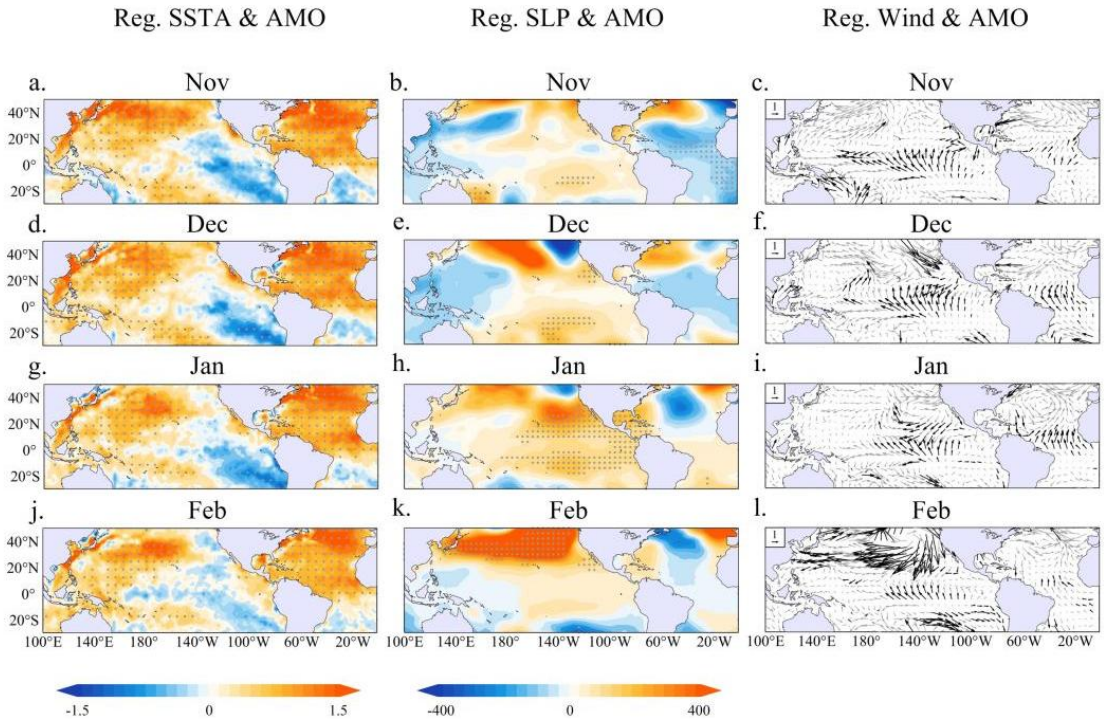


Fig. 8 The footprints of the AMO on Pacific background conditions. Regression maps of (a, d, g, j) SST anomaly (shading; °C), (b, e, h, k) SLP (hPa), and (c, f, i, l) surface wind vectors (m s^{-1}) against the normalized AMO index during 1940–2023, shown for November (a–c), December (d–f), January (g–i), and February (j–l). Stippling indicates the regression coefficients that are statistically significant at the 95% confidence level.

353 The variability in Pacific background state further reshapes the spatial configuration
354 of ENSO. Figure 9b presents the longitude-time evolution of the 21-year running
355 interannual standard deviation (STD) of winter tropical Pacific SST (5° S-5° N). Notably,
356 during periods P1 (1940-1962) and P3 (1999-2014), both the annual STD maxima and
357 their mean values are anchored over the central Pacific. In sharp contrast, during period
358 N1 (1963-1998), these maxima shift decisively eastward. These findings are consistent
359 with previous studies: a positive AMO favors the formation of central Pacific (CP)-type
360 El Niño (Yu et al. 2015; Chung et al. 2013), whereas a negative AMO favors eastern
361 Pacific (EP)-type El Niño (Guo et al. 2024). Mechanistically, a positive AMO steepens
362 the climatological zonal SST gradient across the tropical Pacific, which shifts ENSO-
363 induced convection and the associated atmospheric response westward, ultimately
364 displacing the centre of ENSO SST anomaly in the same westward direction.

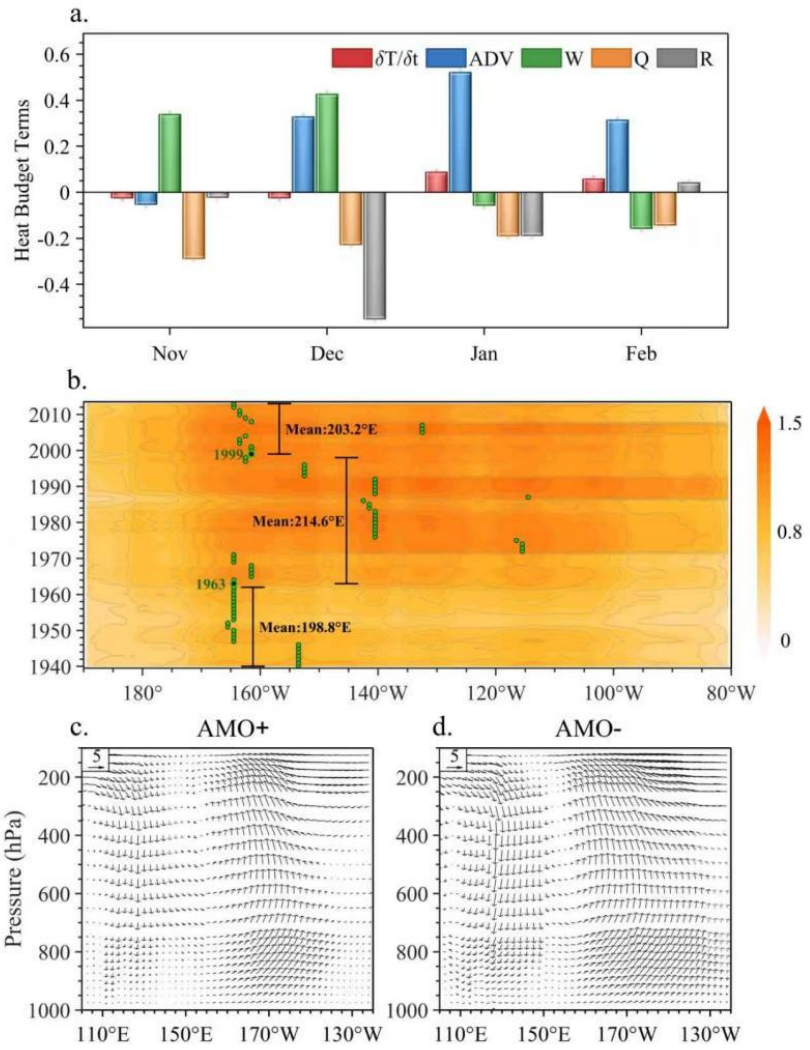


Fig. 9 (a) Comparison of November–February (NDJF) heat budget terms (δT/δt, ADV, W, Q, R; units: °C month^{-1}) averaged over the tropical Pacific (125–150°E, 5°S–5°N) for the period 1940–2010. (b) Hovmöller diagram of the 21-year sliding winter SST standard deviation (STD; °C) averaged over 5°S–5°N during 1940–2018. The positions of annual maximum variability are marked by green points, and the AMO phase-mean are indicated by black lines. (c, d) Anomalous zonal divergent wind (m s^{-1}) and vertical pressure velocity (Pa s^{-1}) averaged over 20°S–20°N (1940–2018) during different AMO phases. The vertical velocity anomalies are multiplied by –1000. Black vectors indicate anomalies significant at the 95% confidence level, while gray vectors denote those that do not pass the significance test.

375 The shift in ENSO spatial pattern further drives the zonal migration of the Pacific
376 Walker circulation. Figure 9c and d shows the composite vertical structure of meridional
377 divergent wind and vertical pressure velocity (5° S-5° N) during the mature phases of El
378 Niño under different AMO phases. During negative AMO phases, the ascending branch
379 of the anomalous Walker circulation extends broadly from 170° E to 130° W, exhibiting
380 an eastward-displaced and expansive structure. In contrast, during positive AMO phases,
381 the ascending branch contracts sharply westward to the 170° E-150° W band (narrowed
382 by approximately 20°), with the descending branch over the western Pacific shifting
383 accordingly. This westward shift, driven by the strengthened zonal SST gradient and
384 anomalous easterlies, pulls the ENSO convective centre westward. In turn, the WNPAC
385 also shifts westward, triggering an anomalous anticyclonic oceanic gyre over the SCS.
386 Through horizontal heat advection, this anticyclonic gyre contributes to the warming of
387 the NSCS shelf. Conversely, during negative AMO phases, the eastward shifted ENSO
388 convection displaces the WNPAC eastward; consequently, the resulting anticyclonic gyre
389 over the SCS no longer covers the NSCS shelf, precluding the occurrence of significant
390 warming there.

391 **3.4** ***Empirical prediction model with AMO-phase-dependent Niño indices***

392 Given the strong remote control exerted by the AMO on the multidecadal variability
393 of the teleconnection between El Niño and NSCS shelf winter SST, this relationship
394 provides a promising basis for developing a predictive framework. However, traditional
395 linear fitting methods underestimate the multidecadal fluctuation of the teleconnection
396 between El Niño and NSCS shelf winter SST, potentially due to their inherent limitation
397 in representing low-frequency variability. Therefore, we employ a 3-year sliding window

fitting method that is more effective in capturing interdecadal signals, with different Niño indices serving as predictors under distinct AMO phases (Fig. 10). The proposed method exhibits notable predictive skill, successfully capturing the observation result of NSCS shelf winter SST influenced by El Niño during different AMO phases. The Niño-4 index performs better than the Niño-3.4 index under positive AMO, whereas the Niño-3 index performs better under negative AMO (Table 1). During the positive AMO phase, moving window fitting with Niño-4 index yields an RMSE of 0.18, representing a 26% improvement over the Niño-3.4 index (0.25). During negative AMO, Niño-3 index based fitting (0.25) outperforms Niño-3.4 index (0.27) by 10% . This phase-dependent performance for Niño index indicates that AMO modulates the spatial pattern of ENSO. Under a positive AMO phase, ENSO-related convection and warming are displaced westward, rendering Niño 4 a more effective predictor of winter SST over the NSCS shelf. Under a negative AMO phase, ENSO variability shifts eastward, making Niño 3 the more relevant predictor.

Table 1 Root mean square error (RMSE) and improvement rates of moving-window linear fits for different Niño indices across AMO phases.

Time	Index	RMSE（Moving Window Fit）	Optimization Rate (vs Niño3.4, %)
P1（1940-1962）	Niño-4	0.1823	26.11%
	Niño-3.4	0.2465	
N1（1963-1998）	Niño-3	0.2467	9.29%
	Niño-3.4	0.2721	
P2（1999-2023）	Niño-4	0.2075	16.33%
	Niño-3.4	0.2480	

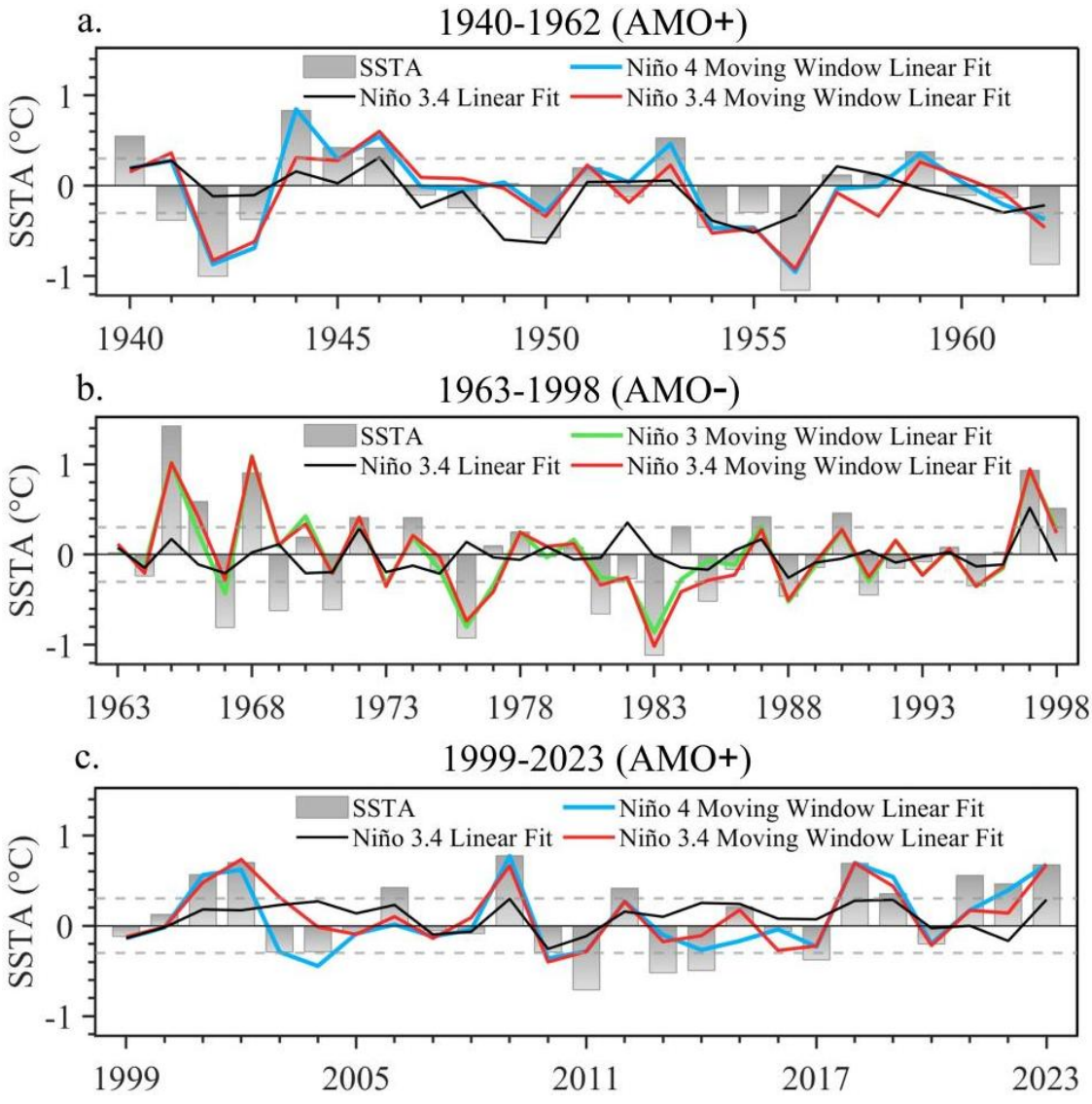


Fig. 10 Prediction of SST anomalies over the NSCS shelf. Time series of observed NSCS shelf winter SST anomalies (gray bars; °C) from HadISST dataset, overlaid with: the linear fit of the Niño-3.4 index (black line), the moving-window linear fit of the Niño-3.4 index (red line), the moving-window linear fit of the Niño-3 index (green line, middle panel), and the moving-window linear fit of the Niño-4 index (blue line, top and bottom panels). Results are shown for three distinct AMO phases: (a) the first positive AMO phase (1940-1962), (b) the negative AMO phase (1963-1998), and (c) the second positive AMO phase (1999-2023).

4. Summary and discussion

Observational analysis suggests that the teleconnection between El Niño and NSCS shelf winter SST exhibits pronounced non-stationary behavior over multidecadal time scales, primarily governed by the remote AMO. Positive AMO amplifies the El Niño–NSCS shelf winter SST teleconnection, while negative AMO attenuates this relationship, and this feature is consistently robust across five independent datasets. The modulation of AMO on the background condition in the tropical Pacific serves as the primary tropical pathway governing the teleconnection between El Niño and NSCS shelf winter SST. Positive-phase AMO-related Atlantic SST warming reorganizes the zonal structure of the Pacific Walker circulation, inducing a distinct west-warm and east-cold thermal dipole across the tropical Pacific, and such zonal thermal contrast is predominantly driven by anomalous zonal oceanic heat advection. This zonal thermal contrast is further amplified through Bjerknes feedback, shifting the center of ENSO westward. In response, the WNPAC shifts westward, thereby inducing significantly positive SST anomalies over the NSCS shelf that arise predominantly from horizontal oceanic heat advection. Based on this dynamical framework, regional climate prediction for the NSCS shelf should account for AMO-induced shifts in ENSO convective centers, thereby necessitating the adoption of distinct ENSO indices. The Niño-4 index is more suitable under positive AMO phases, whereas the Niño-3 index performs better during negative AMO phases; both demonstrate markedly superior predictive skill relative to the conventional Niño-3.4 index.

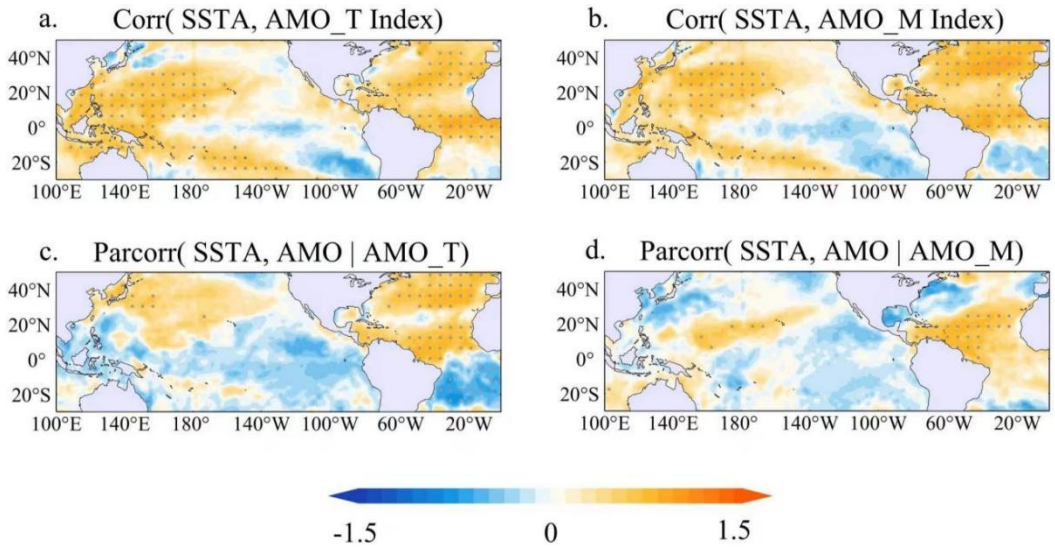


Fig. 11 Correlation maps of Pacific background conditions with different part of AMO. (a) Correlation coefficients between Pacific and Atlantic SST anomalies and the normalized tropical component (5°S-5°N) of AMO index (AMO_T, tropical pathway). (b) Correlation coefficients between Pacific and Atlantic SST anomalies and the normalized mid-latitude component (30-50°N) of AMO index (AMO_M, mid-latitude pathway). (c) Partial correlation coefficients between Pacific and Atlantic SST anomalies and the AMO index, after removing the influence of the AMO_T index. (d) Partial correlation coefficients between Pacific and Atlantic SST anomalies and the AMO index, after removing the influence of the AMO_M index. Stippling indicates regions where the correlation/partial correlation is statistically significant at the 95% confidence level.

Notably, AMO imprints upon tropical Pacific background conditions extend beyond equatorial tropical teleconnection pathways, and such mid-latitude interbasin atmospheric linkage has been widely documented in prior research (Barcikowska et al. 2017; Li et al. 2019; Wang et al. 2025b). During the positive AMO phase, mid-latitude Atlantic SST warming excites an anomalous mid-latitude North Pacific anticyclone via atmospheric bridges. Driven by positive wind-evaporation-SST (WES) feedback (Shang and Philander

1994), this circulation anomaly further amplifies sea surface warming across the subtropical North Pacific (Sun et al. 2017). Subsequently, such subtropical North Pacific thermal anomalies propagate equatorward and lead to sea surface warming over the tropical western Pacific through SST–sea level pressure–cloud–longwave radiation feedback (Wang et al. 2025b). To further clarify the combined effects of these two teleconnection pathways, correlation and partial correlation analyses are conducted (Fig. 11). Correlation analyses reveal that both the tropical component of AMO (AMO_T, 5°S–5°N) (Fig. 11a) and the mid-latitude component of AMO (AMO_M, 30°–50°N) (Fig. 11b) can induce SST warming in the tropical western Pacific. The tropical AMO component exhibits a closer linkage to western Pacific SST anomalies than its mid-latitude counterpart. Partial correlation analyses further show that when the tropical signal is removed from the full AMO index, the correlation with western Pacific SST declines markedly and even turns negative (Fig. 11c). In contrast, after excluding the mid-latitude AMO signal, the correlation also weakens yet remains weakly positive (Fig. 11d). These findings suggest that tropical and mid-latitude AMO teleconnection pathways jointly shape western Pacific SST variability, with the tropical pathway exerting dominant dynamical control. During the positive AMO phase, western Pacific SST warming critically drives the westward displacement of ENSO convective centers and subsequent westward shift of the WNPAC, thereby inducing anomalous winter SST warming over the NSCS shelf. A schematic diagram summarizing the dual dynamical mechanisms is illustrated in Figure 12.

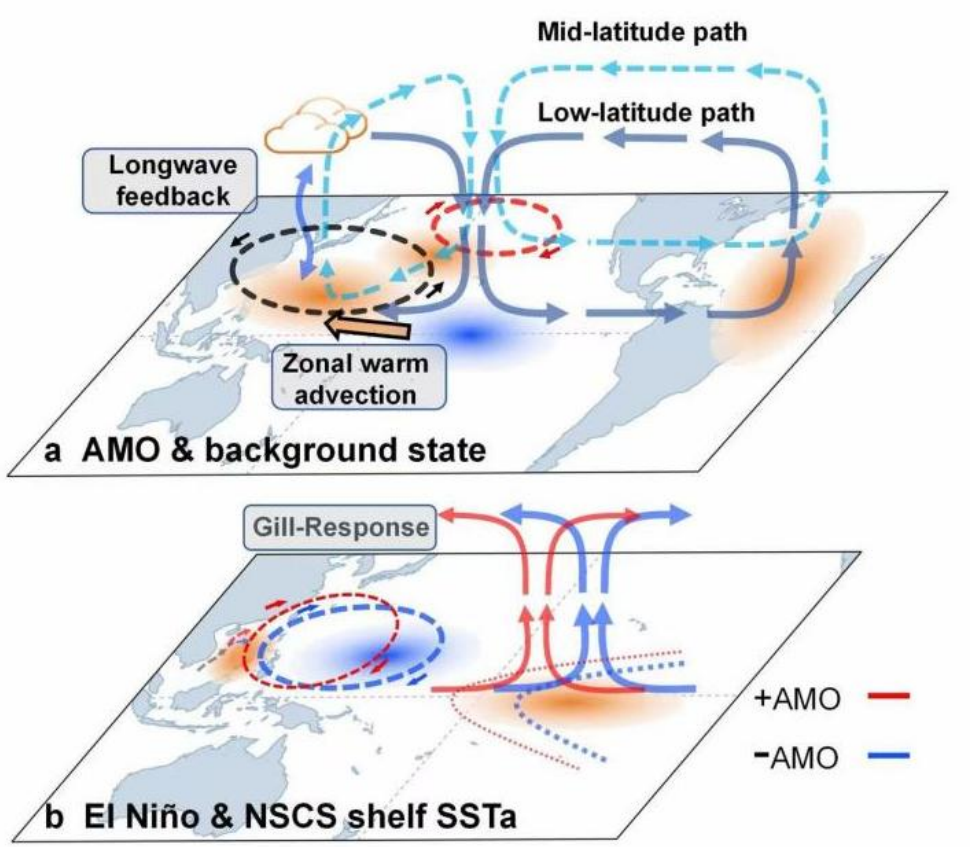


Fig. 12 Schematic of AMO modulation of Pacific background state and the teleconnection between El Niño and NSCS shelf winter SST. (a) Positive AMO phase affects the Pacific background state via tropical (dark blue) and mid-latitude (light blue) pathways. Shadings denote positive (orange) and negative (blue) SST anomalies. Dashed circles represent anomalous anticyclones (red) and cyclones (black). Blue vertical arrows indicate longwave radiation positive feedback, and orange arrows denote equatorial zonal heat advection. (b) Different AMO phases correspond to distinct ENSO patterns and associated WNPAC anomalies. Red and blue represent positive and negative AMO phases, respectively.The dashed line over the NSCS indicates the direction of local zonal heat advection.

Nevertheless, a key limitation of this study is that statistical partial correlation analysis alone cannot definitively identify dynamical causal relationships. While observational datasets support the independent characteristics of the tropical and mid-latitude pathways, additional numerical modelling experiments are essential to verify the

497 physical robustness of each teleconnection channel. Subsequent research can adopt
498 idealized AMO forcing simulations across the Coupled Model Intercomparison Project
499 Phase 6 (CMIP6) multimodel ensemble to independently validate the contributions of the
500 two distinct pathways. Furthermore, targeted numerical experiments focusing on the
501 WNPAC are needed to quantitatively compare the amplitude and spatial displacement of
502 atmospheric circulation responses driven by distinct oceanic thermal forcings. These
503 investigations will elucidate dynamical processes of AMO-induced Pacific–Asian inter-
504 basin dual-pathway linkages, and lay an essential foundation for more reliable regional
505 climate prediction and long-term projection under global warming.

506 ## REFERENCES

507 Barcikowska MJ, Knutson TR, Zhang R (2017) Observed and Simulated Fingerprints of
508 Multidecadal Climate Variability and Their Contributions to Periods of Global SST
509 Stagnation. J Clim 30:721–737. https://doi.org/10.1175/JCLI-D-16-0443.1

510 Box GEP, Jenkins GM (2010) Time series analysis : forecasting and control[J]. J Time
511 Ser Anal 31. https://doi.org/10.1111/j.1467-9892.2009.00643.x

512 Carton JA, Giese BS (2008) A Reanalysis of Ocean Climate Using Simple Ocean Data
513 Assimilation (SODA). Mon Weather Rev 138:2999–3017.
514 https://doi.org/10.1175/2007MWR1978.1

515 Chung PH, Li T (2013) Interdecadal relationship between the mean state and El Niño
516 types. J Clim 26:361–379. https://doi.org/10.1175/JCLI-D-12-00106.1

517 Dai AG, Fyfe JC, Xie SP, Dai XG (2015) Decadal modulation of global surface
518 temperature by internal climate variability. Nat Clim Change 5:555–559.
519 https://doi.org/10.1038/nclimate2605

520 Duan Q, Wang TT, Zhang YH, Du Y (2025) Decadal Linkage of Sea Level Anomalies
521 Between the South China Sea and Western Tropical Pacific. J Geophy Res Oceans
522 130, e2024JC021618. https://doi.org/10.1029/2024JC021618
523 Durbin J, Koopman SJ (2012) Time Series Analysis by State Space Methods. Oxford
524 University Press 488pp.
525 https://doi.org/10.1093/acprof:oso/9780199641178.001.0001
526 Enfield DB, Mestas-Nuñez AM, Trimble PJ (2001) The Atlantic multidecadal oscillation
527 and its relation to rainfall and river flows in the continental U.S. Geophys Res Lett
528 28:2077–2080. https://doi.org/10.1029/2000GL012745
529 Gill AE (1980) Some simple solutions for heat-induced tropical circulation. Q J R
530 Meteorol Soc 106:447–462. https://doi.org/10.1002/qj.49710644905
531 Gong YH, Li T, Chen L (2020) Interdecadal modulation of ENSO amplitude by the
532 Atlantic multi-decadal oscillation (AMO). Clim Dyn 55:2689–2702.
533 https://doi.org/10.1007/s00382-020-05408-x
534 Guo XY, Xu HM, Ma J, Deng JC (2024) Asymmetric modulation of the Atlantic
535 Multidecadal Oscillation on ENSO amplitude. Clim Dyn 63:215.
536 https://doi.org/10.1007/s00382-025-07688-7
537 Hersbach H, Coauthors (2020) The ERA5 Global Reanalysis. Q J R Meteorol Soc
538 146:1999–2049. https://doi.org/10.1002/qj.3803
539 Huang BY, Coauthors (2017) Extended Reconstructed Sea Surface Temperature version
540 5 (ERSSTv5), Upgrades, validations, and intercomparisons. J Clim 30:8137-8155.
541 https://doi.org/10.1175/JCLI-D-16-0836.1

542 Kaplan A, Cane MA, Kushnir Y, Clement AC, Blumenthal MB, Rajagopalan B (1998)
543 Analyses of global sea surface temperature 1856–1991. J Geophys Res 103:18567–
544 18589. https://doi.org/10.1029/97JC01736
545 Klein SA, Soden BJ, Lau NC (1999) Remote sea surface temperature variations during
546 ENSO: Evidence for a tropical atmospheric bridge. J Clim 12:917–932.
547 https://doi.org/10.1175/1520-0442(1999)0122.0.CO;2
548 Knight JR, Folland CK, Scaife AA (2006) Climate impacts of the Atlantic Multidecadal
549 Oscillation. Geophys Res Lett 33:L17706. https://doi.org/10.1029/2006GL026242
550 Kucharski F, Kang IS, Keenlyside NS, Chang P, Farneti R, Nnamchi HC, Li JP (2015)
551 Thermodynamic controls of the Atlantic Niño. Nat Commun 6:8985.
552 https://doi.org/10.1038/ncomms9895
553 Li JP, Zheng F, Sun C, Feng J, Wang J (2019) Pathways of Influence of the Northern
554 Hemisphere Mid-high Latitudes on East Asian Climate: A Review Adv Atmos Sci
555 36:902–921. https://doi.org/10.1007/s00376-019-8236-5
556 Lin Y, Gan J, Cai Z, Quan Q, Zu T, Liu Z (2024) Coherent Interannual–Decadal Potential
557 Temperature Variability in the Tropical-North Pacific Ocean and Deep South China
558 Sea. Geophys Res Lett 51: e2023GL106256. https://doi.org/10.1029/2023GL106256
559 Liu FY, Zhang WJ, Jin FF. Hu SQ (2021) Decadal Modulation of the ENSO–Indian
560 Ocean Basin Warming Relationship during the Decaying Summer by the
561 Interdecadal Pacific Oscillation. J Clim 34:2685–2699. https://doi.org/10.1175/JCLI-
562 D-20-0457.1

563 Liu QY, Jiang X, Xie SP. Liu WT (2004) A Gap in the Indo-Pacific Warm Pool Over the
564 SCS in Boreal Winter:Seasonal Development and Interannual Variability. J Geophy
565 Res Oceans 109:C07012. https://doi.org/10.1029/2003JC002179
566 Luongo MT, Xie SP, Eisenman IS, Sun T, Peng QH (2025) How the Subsurface Tropical
567 Pacific Responds to Subtropical Surface Cooling: Implications for Cross-Equatorial
568 Transport. J Clim 38:3313–3331. https://doi.org/10.1175/JCLI-D-24-0440.1
569 McGregor S, Stuecker MF, England MH, Merrifield M, Jin FF, Chikamoto Y,
570 Timmermann A (2014) ENSO-driven interhemispheric Pacific mass transports. J
571 Geophys Res Oceans 119:6221–6237. https://doi.org/10.1038/nclimate2330
572 Percival DB, Walden AT (1993) Spectral Analysis for Physical Applications: Multitaper
573 and Conventional Univariate Techniques. Cambridge University Press 583pp.
574 https://doi.org/10.1017/CBO9780511622762
575 Rayner NA, Horton DE, Folland CK, Alexander LV, Rowell DP, Kent EC, Kplan A
576 (2003) Global analyses of sea surface temperature, sea ice, and night marine air
577 temperature since the late nineteenth century. J Geophys Res 108:4407.
578 https://doi.org/10.1029/2002JD002670
579 Reynolds RW, Smith TM, Liu CY, Chelton DB, Casey KS, Schlax MG (2007) Daily
580 high-resolution-blended analyses for sea surface temperature. J Clim 20:5473–5496.
581 https://doi:10.1175/JCLI-D-14-00293.1
582 San SC, Tseng YH, Ding RQ, Lorenzo ED (2024) A key role of off-equatorial subsurface
583 temperature anomalies in Tropical Pacific Decadal Variability. Npj Clim Atmos Sci
584 7:109. https://doi.org/10.1038/s41612-024-00643-z

585 Schrunner S, Pishrobat P, Janssen J, Jenul A, Cao JG, Ameli AA, Welch WJ (2023) A
586 Gaussian Sliding Windows Regression Model for Hydrological Inference. J R Stat
587 Soc Ser C Appl Stat 74:946-968. https://doi.org/10.1093/jrsssc/qlaf009
588 Seow MXC, Tozuka T (2019) Ocean thermodynamics behind the asymmetry of
589 interannual variation of South China Sea winter cold tongue strength. Clim Dyn
590 52:3241–3253. https://doi.org/10.1007/s00382-018-4320-2
591 Shang PX, Philander SGH (1994) A coupled ocean-atmosphere model of relevance to the
592 ITCZ in the eastern Pacific. Tellus Series A 46:340–350.
593 https://doi.org/10.3402/tellusa.v46i4.15484
594 Shi M, Chen C, Xu Q, Lin H, Liu G, Wang H, Wang F, Yan J (2002) The Role of
595 Qiongzhou Strait in the Seasonal Variation of the South China Sea Circulation. J
596 Phys Oceanogr 32:103–121. https://doi.org/10.1175/1520-
597 0485(2002)032<0103:TROQSI>2.0.CO;2
598 Smith KE, Burrows MT, Hobday AJ, Gupta AS, Moore PJ, Thomsen M, Wernberg T,
599 Smale DA (2021) Socioeconomic impacts of marine heatwaves: Global issues and
600 opportunities. Science 374:eabj3593.
601 https://www.science.org/doi/10.1126/science.abj3593
602 Sun C, Kucharski F, Li JP, Kang IS, Ding RQ (2017) Western tropical Pacific
603 multidecadal variability forced by the Atlantic multidecadal oscillation. Nat
604 Commun 8:15998. https://doi.org/10.1038/ncomms15998
605 Tang YL, Huangfu JL, Huang RH, Chen W (2020) Surface Warming Reacceleration in
606 Offshore China and Its Interdecadal Effects on the East Asia-Pacific Climate. Sci Re,
607 10:14811.https://doi.org/10.1038/s41598-020-71862-6

608 Torrence C, Compo GP (1998) A Practical Guide to Wavelet Analysis. Bull Amer
609 Meteor Soc 79:61–78. https://doi.org/10.1175/1520-
610 0477(1998)079<0061:APGTWA>2.0.CO;2
611 Wang B, Wu RG, Fu X (2000) Pacific–East Asian teleconnection: How does ENSO
612 affect East Asian climate? J Clim 13:1517–1536. https://doi.org/10.1175/1520-
613 0442(2000)013<1517:PEATHD>2.0.CO;2
614 Wang CZ, Wang WQ, Wang DX, Wang Q (2006) Interannual variability of the South
615 China Sea associated with El Niño. J Geophy Res 111:C03023.
616 https://doi.org/10.1029/2005JC003333
617 Wang Q, Zhang B, Zeng L, He Y, Wu Z,Chen J (2022) Properties and Drivers of Marine
618 Heat Waves in the Northern South China Sea. J Phys Oceanogr 52:917–927.
619 https://doi.org/10.1175/JPO-D-21-0236.
620 Wang Z, Wu R (2021) Individual and Combined Impacts of ENSO and East Asian
621 Winter Monsoon on the South China Sea Cold Tongue Intensity. Clim Dyn 56:3995–
622 4012, https://doi.org/10.1007/s00382-021-05682-3
623 Wang ZY, Yao SQ, Qiu MP, Wang YY, Zhang GS, Dong WJ, Sun RL (2025) Inter-
624 Basin Teleconnection of the Atlantic Multidecadal Oscillation and Interdecadal
625 Pacific Oscillation in Modulating the Decadal Variation in Winter SST in the South
626 China Sea. J Mar Sci Eng 13:2355. https://doi.org/10.3390/jmse13122355
627 Wang ZY, Wang YY, Qiu MP, Ma XH, Cheng KL, Yao SQ, Zhang YM, Dong WJ, Liu
628 X, Han Y, Shi XR (2025) Modulation of the Pacific Decadal Oscillation on the
629 Weakening of the South China Sea Winter Cold Tongue During the Mature Phase of
630 El Niño. Adv Meteorol 16:1687-9317. https://doi.org/10.1155/adme/6329984

631 Wang ZY, Wang YY, Qiu MP, Zhang YM, Zhang GS, Dong WJ (2025) PDO-Modulated
632 ENSO Impact on Southern South China Sea Winter SST: Multi-Anticyclone Synergy.
633 J Mar Sci Eng 13:1741. https://doi.org/10.3390/jmse13091741
634 Wernberg TD, Smale A, Tuya F, Thomsen MS, Langlois TJ, Bettignies T, Bennett S,
635 Rousseaux CS (2013) An extreme climatic event alters marine ecosystem structure in
636 a global biodiversity hotspot. Nat Clim Change 3:78–82.
637 https://doi.org/10.1038/nclimate1627
638 Wong LA, Chen JC, Xue H, Dong LX, Su JL, Heinke G (2003) A model study of the
639 circulation in the Pearl River Estuary (PRE) and its adjacent coastal waters: 1.
640 Simulations and comparison with observations. J Geophys Res 108:3156.
641 https://doi.org/10.1029/2002JC001451
642 Wu B, Zhou TJ, Li T (2017) Atmospheric dynamic and thermodynamic processes driving
643 the western North Pacific anomalous anticyclone during El Niño. Part II: Formation
644 processes. J Clim 30:9637–9650. https://doi.org/10.1175/JCLI-D-16-0495.1
645 Wyrtki K (1961) Physical Oceanography of the Southeast Asian Waters; Naga Report.
646 UC San Diego: Library – Scripps Digit Collec 447–462.
647 https://doi.org/10.1002/qj.49710644905
648 Xiao FA, Wang DX, Leung MYT (2020) Early and extreme warming in the South China
649 Sea during 2015/2016:Role of an unusual Indian Ocean dipole event. Geophy Res
650 Lett 47:e2020GL089936. https://doi.org/10.1029/2020GL089936
651 Xue JQ, Luo JJ, Zhang WJ, Yamagata T (2022) ENSO–IOD inter-basin connection is
652 controlled by the Atlantic Multidecadal Oscillation. Geophys Res Lett
653 49:e2022GL101571. https://doi.org/10.1029/2022GL101571

654 Xue JQ, Zhang WJ, Zhang YT, Luo JJ, Hua HL, Sun C, Yamagata T (2025) Interdecadal
655 modulation of Ningaloo Niño/Niña strength in the Southeast Indian Ocean by the
656 Atlantic Multidecadal Oscillation. Nat Commun 16:1966.
657 https://doi.org/10.1038/s41467-025-57160-7
658 Xu M, Xu HM, Ma , Deng JC (2023) Modulation of Atlantic Multidecadal Oscillation on
659 ENSO-East Asian early summer monsoon connection: role of a tropical pathway.
660 Clim Dyn 61:4301–4318. https://doi.org/10.1007/s00382-023-06811-w
661 Yu JY, Kao PK, Paek H, Hsu HH, Hung CW, Lu MM, An S (2015) Linking emergence
662 of the central Pacific El Niño to the Atlantic multidecadal oscillation. J Clim 28:651–
663 662. https://doi.org/10.1175/JCLI-D-14-00347.1
664 Zhang RH, Sumi A, Kimoto M (1996) Impact of El Niño on the east Asian monsoon. J
665 Meteorol Soc of Jpn 74:49–62. https://doi.org/10.2151/jmsj1965.74.1_49
666 Zhang Y, Zeng LL, Wang Q, Geng XB, Liu CJ, Shi R, Liu N, Wang WP, Wang DX
667 (2021) Seasonal variation in the three-dimensional structures of coastal thermal front
668 off western Guangdong. Acta Oceanol Sin 40:88–99. https://doi.org/10.1007/s13131-
669 021-1739-9
670 Zhao CX, Geng X, Zhang WJ, Qi L (2022) Atlantic Multidecadal Oscillation modulates
671 ENSO atmospheric anomaly amplitude in the tropical Pacific. J Clim 35:3891–3903.
672 https://doi.org/10.1175/JCLI-D-21-0603.1

673 **Funding** the Natural Science Foundation of Hainan Province (NO.426MS0193),
674 National Natural Science Foundation of China (NO.42266005), Scientific Research
675 Foundation of Hainan Tropical Ocean University (NO.RHDRC202322,RHDRC202103)

676 and Special Program of Hainan Province for Academician Innovation Platform (NO.
677 YSPTZX202507).

678 **Data availability** The monthly SST used in this study is the (HadISST at
679 https://www.metoffice.gov.uk/hadobs/hadisst/. The ERSST data were provided by the
680 U.S. National Oceanic and Atmospheric Administration and are available at
681 https://www1.ncdc.noaa.gov/pub/data/. The OISST data set were provided at
682 https://gdex.ucar.edu/dataset/158_asphilli/file.html. The Kaplan SST data were provided
683 by the NOAA PSL, Boulder, Colorado, USA, and can be accessed at
684 http://psl.noaa.gov/data/gridded/data.kaplan_sst.html. The monthly mean SLP, surface
685 wind, surface heat flux, total precipitation, SST are sourced from the ERA5 reanalysis
686 provided by the ECMWF at https://www.ecmwf.int/en/forecasts/datasets/reanalysis-
687 datasets/era5. The monthly mean oceanic currents and mixed layer depth data are sourced
688 from the SODA system v2.2.4 at http://apdrc.soest.hawaii.edu/datadoc/soda_2.2.4.php.

689 **Declarations**

690 **Conflict of interest** The authors declare that they have no conflict of interest.